Int. J. Electrochem. Sci., 8 **(2013)** 11186 - 11200

International Journal of
ELECTROCHEMICAL
SCIENCE
www.electrochemsci.org

Sequential Analysis of Electrochemical Properties of B–Tricalcium Phosphate/Chitosan Coatings Obtained on 316L Stainless Steel

A. Mina[1], *J. C. Caicedo*[1], *W. Aperador*[2]

[1]Powder Metallurgy and Processing of Solid Recycling Research Group,
Universidad del Valle, Cali-Colombia
[2]Departament of Engineering, Universidad Militar Nueva Granada, Bogotá-Colombia

Received: 19 June 2013 / *Accepted:* 28 July 2013 / *Published:* 20 August 2013

Biocompatible coatings of β–Tricalcium phosphate-Chitosan were deposited on 316L stainless steel (316L SS) substrates via electrodeposition. The aim of this work is determinate the electrochemical behavior of AISI 316L substrates by using β–Tricalcium phosphate-Chitosan as a protective coating. The coatings were characterized by Fourier Transformed Infrared spectroscopy (FTIR spectroscopy) that showed bands associated to β–Tricalcium phosphate (β–TCP) and Chitosan (Ch). By using electrochemical impedance spectroscopy with (EIS) and Tafel curves it was possible to determinate electrochemical behavior of 316L SS substrates coated with β–TCP-Ch in Hanks solution (HBSS). Dispersive X-ray analysis (EDX) and Scanning electron microscopy (SEM) were performed to analyze chemical changes and morphological surfaces changes on β–TCP-Ch coatings due to the reaction in HBSS/β–TCP-Ch surface coatings interface. Electrochemical behavior in HBSS indicates the coatings may be a promising material for biomedical industry application for temporal invasive prosthesis.

Keywords: Electrodeposition, β–Tricalcium phosphate (β–TCP), Chitosan (Ch), Electrochemical properties, Hanks solution (HBSS).

1. INTRODUCTION

Biocompatible materials to decrease healing times and rise fixation into bone and prosthesis interface are the challenge that materials engineers face daily due to it is necessary to guarantee a better life quality for patients though more effective treatments. Medicine and materials engineering has focused in develop novel materials to aim medicine and biomedical industry. AISI 316L stainless steel is widely used in biomedical industry to applications for temporal invasive prosthesis due it has a high content of chromium (Cr), this element gives corrosion resistance due to passivity. However this

passive film cannot avoid pitting corrosion in AISI 316L stainless steel [1] for this reasons the AISI 316L stainless steel materials cannot be used for permanent biomedical devices. Materials engineering has focused in develop novel materials as coatings to improve electrochemical behavior of metallic substrates to aim medicine and biomedical industry [1]. Ceramic materials as hydroxyapatite (HA) and β-tricalcium phosphate (β-TCP) have been studied because they have excellent biological properties due to its chemical composition, which are very similar to the mineral component of the bone [2–5]. β-Tricalcium phosphate is a ceramic material that has been used as bone substitute, bone graft, drugs delivery systems and coatings due to biocompatibility, bioactivity and osteoconductivity behavior [6]. The literature present that Chitosan is a natural cationic polysaccharide it is produced by alkaline N-deacetylation of chitin, a constituent of the exoskeleton from crabs and squid, mainly this polymer has been used to improve integration of implant and bone regeneration due to its bioactive characteristics, such as cell proliferation [7]. Yokogata et al, [8] studied coatings of Calcium phosphates with Chitin and Chitosan, it was found a growth of thin films of calcium phosphate due to hydrolysis of functional group PO_4 in contact with Fetal Bovine Serum (FBS). Pang et al, [9] obtained cathodic deposits of HA and Chitosan applying electrochemical techniques, it was showed an increase in polarization resistance values related to the protective nature of the coatings. By using electrodeposition has been possible to deposit biomaterials on metallic substrates, this advance has provided greater advantages in biomedical industry and medicine [9]. In this way the literature present few researches focused on studying the ceramic-polymeric-corrosive phenomenon, therefore, this effect on 316L stainless steel coated with β–TCP-Chitosan has been studied weakly. Taking in account the above the electrochemical (corrosion) effect on steel uncoated and steel coated with β–TCP-Chitosan has not yet been thoroughly studied, due to this electrochemical effect problems can be highly observed in biomedical an human devices steel with industrial application (e.g. femoral stem). This work shows the influence of Chitosan percentage in Chemical, and electrochemical behavior of β–TCP-Ch coatings, in this sense, from electrochemical results β–TCP-Ch coatings could be used as promising material for biomedical industry.

2. EXPERIMENTAL

Cylindrical substrates of AISI 316L SS with 12 mm of diameter and 5 mm of thickness were activated by superficial electrochemical etching by using an acid solution of 1:1:1 HCl, H_2SO_4 H_2O, to improve adhesion characteristics in the substrate-coating interfaces with β-Tricalcium phosphate (β-TCP) and Chitosan (Poly-(1-4)-2-Amino-2-deoxy-ß-D-Glucan) to generate the β-TCP-Chitosan ((β-$Ca_3(PO_4)_2$)-($C_6H_{11}NO_4$)n) coating systems which were deposited via cathodic electrodeposition by using an electrolyte compound by two solutions, first one a β-TCP solution dissolved in ethanol-water solution and the second one was carried out with Chitosan solution dissolved in acetic acid to 2%. TCP-Chitosan coatings were deposited via cathodic electrodeposition with a current density of 260 mA, an agitation velocity of 250 rpm, pH electrolyte of 10.4 and a temperature deposition of 60°C.

The Fourier Transformed Infrared spectroscopy FTIR were recorded in a Shimatzu 8000 FTIR spectrometer and over 500 – 4000 cm^{-1} range. For this, the coatings were extracted from de substrate

and crushed to fine powder. 3% of Kbr, which is transparent to IR radiation, was mixed and compacted with β-TCP-Chitosan coating extracted and crushed, disc for IR absorption spectra measurements were formed by pressing the mixture of powders. The electrochemical behavior under Hanks solution (HBSS) was performed by EIS and Tafel by using model PCI-4 potenciostat-galvanostat, it is compound by a cell with a working electrode of 1-cm^2 exposed area, Ag/AgCl (3.33 M KCl) reference electrode, and platinum wire counter-electrode under a Hanks solution (HBSS) (Table 1). Impedance values were obtained with simulated human temperature of 37±0.2°C and different test times 1h, 24h 48h 168h and 336h in different compositions of β-TCP-Ch coating. For Nyquist plots, frequency sweeps were conducted in the range of 100 kHz to 0.001 Hz using sinusoidal signal amplitude of 10 mV applied to the working electrode (sample) and the reference electrode. Diagrams for Tafel polarization curves were obtained at a sweep speed of 0.125 mV/s in a voltage range of −1000 to 1000 mVAg/AgCl; this voltage range was defined with respect to the open circuit potential (OCP). Prior to beginning the polarization curve procedures, the samples were submerged in the Hanks solution for 30 min to establish the free corrosion potential values (Ecorr) where polarization curve measurements were initiated. The EDX analysis was developed by using a scanning electron microscope JEOL JSM-6490LV to know chemical changes in surface after electrochemical characterization related with the bioactive characteristic of β-TCP-Ch coating in a simulated media as Hanks solution.

Table 1. Chemical composition of commercial Hanks solution [10].

Compound	Concentration (g/l)
NaCl	8
D-Glucose	1
$MgSO_2HPO_4$	0.7
Na_2HPO_4	0.48
KCl	0.4
$NaHCO_3$	0.35
$CaCl_2.H_2O$	0.18
$MgO_2.6H_2O$	0.008
KH_2PO_4	0.006

3. RESULTS AND DISCUSSION

3.1 Analysis by FTIR spectroscopy

The changes in transmittance percentage for each β-TCP-Ch coatings are presented in Figure 1 which shows waves number for each characteristic bond of β-TCP material and Chitosan material in the frequency range 500 – 4000cm^{-1}. The spectrum of β-TCP-Ch coating in different composition for comparison showing congruence in values of wave numbers; According with other authors [10-12], due to combination of β-TCP and Chitosan it can be possible to find vibration bands associated to both

materials, in this sense it could be a constructive interference. Vibration bands associated to β-TCP are described bellow; CO_3 blending vibration band between 1482 cm^{-1} and 1424 cm^{-1} was found; at 1038.67 cm^{-1} was observed a vibration band corresponding to tetrahedral structure of PO_4^{-3}, the wave number 875.17 cm^{-1} showed a vibration band corresponding to HPO_4 and finally at 565.19 cm^{-1} there is a blending vibration band which is associated to PO_2. On the other hand, due to Chitosan existence it were found symmetric stretching vibrations band of NH_2 in the region of 3700 cm^{-1} -3500 cm^{-1} overlapping with stretching vibration bands associated to OH^- between 3500 cm^{-1} and 3200 cm^{-1}; also, C-O-H bending vibration bands can be observed between 1300 cm^{-1}-1450 cm^{-1}; Finally, between 1020-1250 cm^{-1} was found vibration bands of primary aliphatic amines (CN).

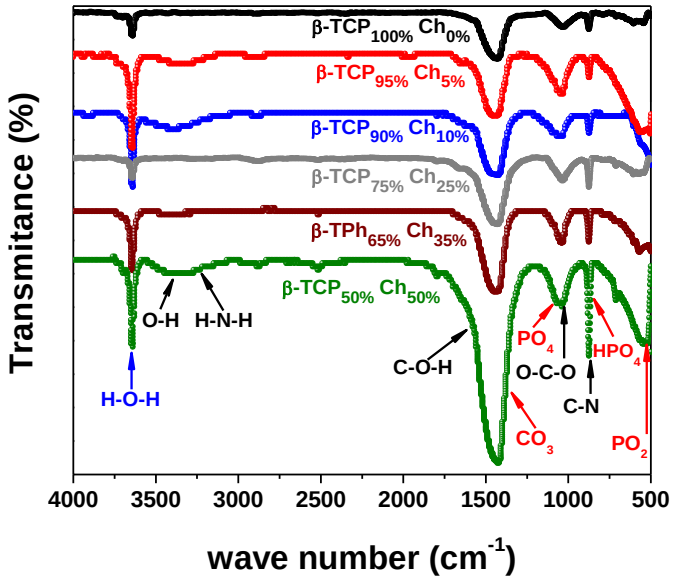

Figure 1. FTIR spectra for β-TCP and β-TCP-Chitosan coatings as function of Chitosan concentration.

FTIR spectra exhibit an increase in transmittance bands when increase Chitosan percentage in β-TCP-Ch coatings as can be seen in Figure 1, in this sense, there are two preferential vibration bands at 3642.72 cm^{-1} and 1450 cm^{-1} which are presented in each FTIR spectra of β-TCP-Ch coating. These two preferential vibration bands are observed in absorbance mode (Fig. 2), it could be observed vibration bands behave as polynomial functions, vibration bands of β-TCP and Chitosan are overlapped so, by using deconvolutions funtions was possible to determinate gaussians signals related with the contributions in absorbance percentage of each material.

Figure 2a shows the deconvolution of Tricalcium phosphate (β-TCP) (β-$Ca_3(PO_4)_2$ with Chitosan ($C_6H_{11}NO_4$)n) such as (TCP_{50}-Ch_{50}) coating where Gaussians signals are associate to CO_3 molecule corresponding to β-TCP material and C-O-H molecule corresponding to Chitosan material, therefore, the deconvolutions show the contribution of each material in the functionalized β-TCP-Chitosan coating. In this sense the

Figure 2b show an increase in absorbance percentage of vibration bands for β-TCP-Ch coatings between 1300-1450 cm^{-1} as function of Chitosan percentage; From

Figure 2b, it can observe an exponential behavior in the absorbance percentage, moreover in the current reseacg it was possible to find that a addition of 50% of Chitosan are closer to saturation percentage of the crystal structure.

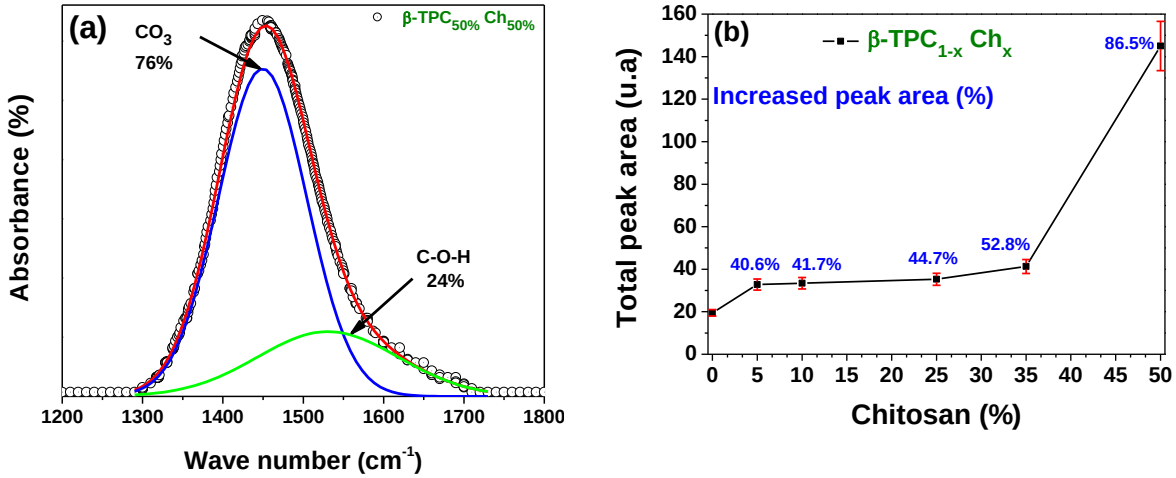

Figure 2. Chemical contribution of β-TCP-Ch coating; (a) deconvolution of β-TCP_{50}-Ch_{50} coating and (b) Increase of vibration bands (total peak area) as function of Chitosan percentage.

3.2 Electrochemical Impedance Spectroscopy analysis

Using electrochemical impedance spectroscopy (EIS) it was possible to observe the Hanks solution effect on the solution/coating interface and subsequently can determinate the electrochemical behavior of β-TCP-Chitosan coatings. AISI 316L stainless steel substrates coated with β-TCP-Chitosan coatings were exposed in the biological solution (Hanks solution) during 1, 24, 42, 168 and 336 hours, to determinate electrochemical stability under biological environment.

Figure 3 presents Nyquist plots of each β-TCP-Ch coating evaluated different exposition times; Nyquist plots exhibit high impedance values of β-TCP-Chitosan coatings comparing with electrochemical response of substrates of AISI 316L stainless steel uncoated.

Nyquist plots show an increase of impedance values while increase exposition times, due to bioactive characteristic of β TCP in biological environments, moreover, β-TCP (β-$Ca_3(PO_4)_2$-Chitosan ($(C_6H_{11}NO_4)n$) or ((Poly-(1-4)-2-Amino-2-deoxy-ß-D-Glucan) coatings provide a protection to metallic substrate in a biological and corrosive environment because the coatings react with ions delivered from Hanks solution (HBSS) (Table 1), therefore, the coatings reduces the corrosion and degradation substrate. On the other hand, with an increase in Chitosan percentage was possible to observe an increase of impedance values in this way, an increase of impedance values suggest an increase in the effect protective of β-$Ca_3(PO4)_2$ - $(C_6H_{11}NO_4)n$ coating due to Chitosan inclusion in the coating [13].

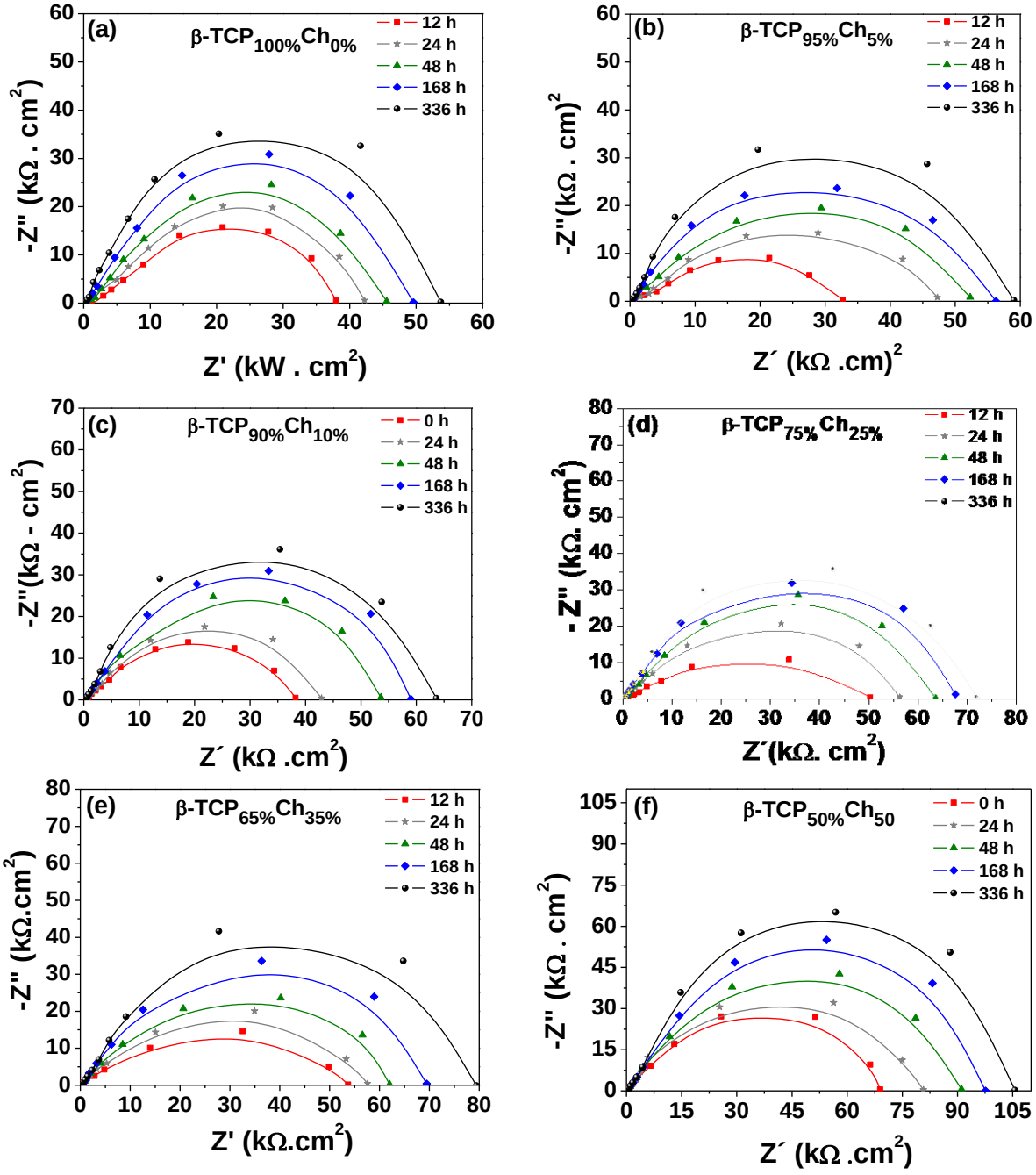

Figure 3. Nyquist plots of the β-TCP-Ch coatings as function of increasing of Chitosan concentration: (a) β-$TCP_{100\%}Ch_{0\%}$, (b) β-$TCP_{95\%}Ch_{5\%}$, (c) β-$TCP_{90\%}Ch_{10\%}$, (d) β-$TCP_{75\%}Ch_{25\%}$, (e) β-$TCP_{65\%}Ch_{35\%}$, and (f) β-$TCP_{50\%}Ch_{50\%}$.

The highest values of impedance of AISI 316L Stainless Steel substrates coated with β-TCP-Chitosan coatings exposed in the biological solution (Hanks solution) are registered in exposition times of 336 hour; Figure 4 presents Nyquist plots of the β-TCP-Chitosan coatings evaluated at 336 hours as function of increasing of Chitosan concentration, increase of impedance values due to ions of Hanks solution are deposited on the surface coating in this way decrease the reaction in the solution/coating

interface in this sense an increase of exposition time suggest a improvement in electrochemical stability of coatings.

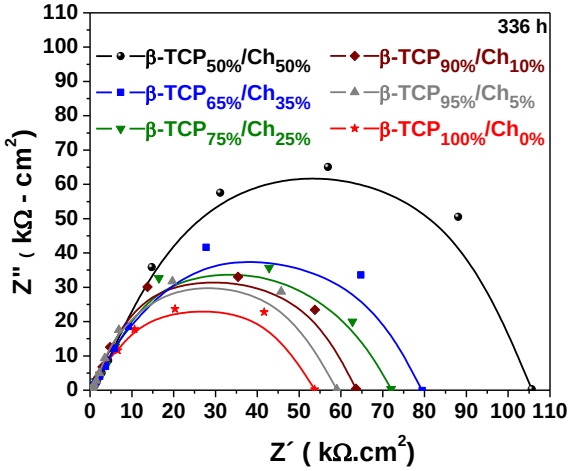

Figure 4. Nyquist plots of the β-TCP-Chitosan coatings evaluated at 336 hours as function of increasing of Chitosan concentration.

Take in account the last discussion, Randles cell can be an approximation of equivalent circuit by using a fitting in experimental data [14]. Equivalent circuit is used to simulate the phenomenon in the interfaces associated with electrochemical assay (interface coating/electrolyte and the interface metallic substrate/coating); these interfaces compose two double layer capacitors in parallel, also electrolyte and coating give resistances to the system due to ions transfer reactions from electrolyte to metal substrate [14, 15]. Figure 5 exhibits the equivalent circuit which contains two capacitor elements that contribute a pseudo-capacitance to the system´s total impedance; the capacitor elements labeled constant phase element (Yel-re; Ydl), are associated to the interfaces of the system, Ydl is associated to interface β-TCP-Chitosan coating /316L stainless steel substrate. and Yel-re is a constant phase element associated to interface HBSS/β-TCP-Chitosan coating Also there are two resistances; (Rel-re; Rdl) associated to resistance between Hanks solution and β-TCP-Chitosan coating and the other one associated to resistance between β-TCP-Chitosan coating and AISI 316L stainless steel substrate resistance.

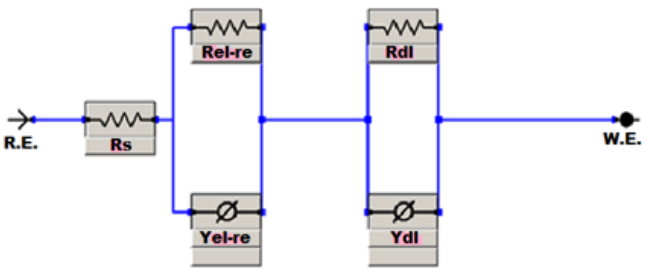

Figure 5. Equivalent circuit used to fit system impedance data.

From impedance values analyzed in the Figure 4 were possible to determinate the polarization resistance behavior as function of Chitosan percentage due to relationship between impedance values and polarization resistance, this graph show an increase in polarization resistance with an increase of Chitosan percentage due to bioactive characteristic of β-TCP in biological environments and the inclusion of Chitosan (polymer material) into β-TCP structure so, this factors promote a effect protective on metallic substrate. Figure 6 presents polarization resistance as function of Chitosan which show an increase in polarization resistance with an increase of Chitosan percentage due to bioactive characteristic of β-TCP in biological environments and the inclusion of Chitosan (polymer material) into β-TCP structure so, this factors promote a protective effect on metallic substrate (stainless steel).

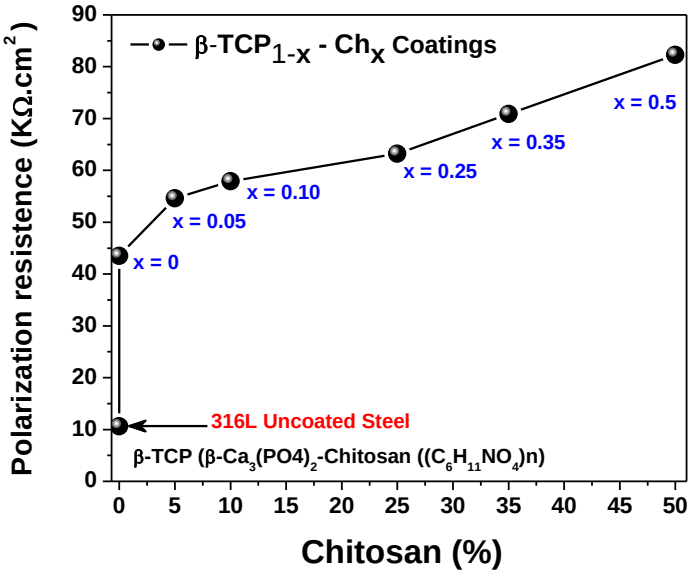

Figure 6. Polarization resistance as function of Chitosan concentration.

3.3 Potentiodinamic polarization analysis

Figure **7** shows the potentiodinamic polarization (Tafel curve) for β-TCP-Ch coating deposited on AISI 316L stainless steel substrate under Hanks solution which show potential as function of current density; Tafel curves show the intersection between the anodic curve and cathodic curve, in this intersection can be possible to obtain current density of corrosion value and potential of corrosion [16]. From Tafel curves shown in Fig 7. it can possible to observe a tendency to achieve more electronegative potentials; in this sense with an increase in Chitosan percentage it is possible to decrease corrosion potential values. This decrease of corrosion potential values are related with the bioactive characteristic of β-TCP (β-$Ca_3(PO_4)_2$ in biological environments and chemical stability of β-TCP (β-$Ca_3(PO_4)_2$-Chitosan (($C_6H_{11}NO_4$)n) coatings as were previously discussed in EIS analysis.

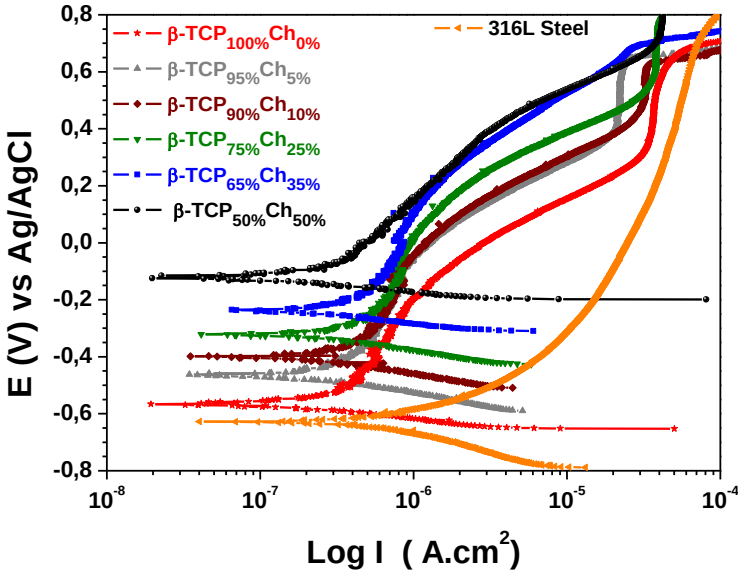

Figure 7. Potentiodinamic polarization (Tafel curves) for AISI 316L stainless steel substrate under Hanks solution and β-TCP-Chitosan coating as function of Chitosan concentration.

From Fig 7. were possible to obtain the anodic and cathodic tafel slopes for each coating so, it was possible analytically determinate the value of corrosion rate by using Stern – Geary [17]:

$$i_{corr} = \frac{\beta_a \beta_c}{\{2.303(\beta_a+\beta_c)\}} * \left[\frac{1}{R_p}\right] \qquad (1)$$

where Rp is the polarization resistance, β_a and β_c are the anodic and cathodic Tafel slopes.

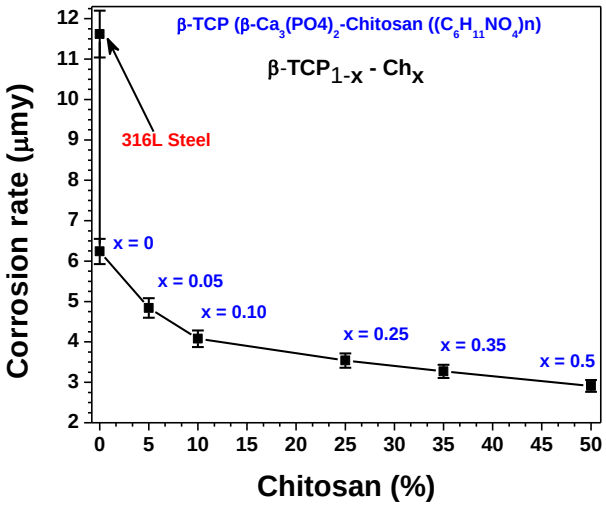

Figure 8. Electrochemical behavior; Corrosion rate as function of Chitosan percentage.

From potential of corrosion values, it was possible demonstrate that increase of Chitosan percentage improve the electrochemical behavior, in this sense the Figure 8 shows a decrease of corrosion rate while increase Chitosan percentage, it show a change of 24.36% in corrosion rate values

of AISI 316L stainless steel substrate comparing with corrosion rate of substrate coated with β-TCP coating, but using β-TCP-Ch coating can be possible obtain an reduction of 52.85% in corrosion rate values. This phenomenon can be explained due to the inclusion of Chitosan (polymer material) with low electrochemical reactivity into β-TCP structure.

From values of polarization resistance it could be possible to determinate a porosity factor according with other authors [18, 19]. The total film porosity factor equation is shown bellow, it correspond to the ratio between the polarization resistance of uncoated substrate and the coated substrate.

$$P = \frac{R_{p,u}}{R_{p,r-u}} \qquad (2)$$

where P is the total coating porosity, $R_{p,\ r-u}$ is the polarization resistance of the uncoated substrate and $R_{p,u}$ is the measured polarization resistance of the coating-substrate system.

Figure **9** presents the porosity factor values obtained replacing the electrochemical values on Eq. (3) for each coating. Porosity factor as function of Chitosan percentage curve suggest that the porosity factor decreases with the increase of Chitosan percentage in relation with widening of vibration bands exposed in Figure 1.

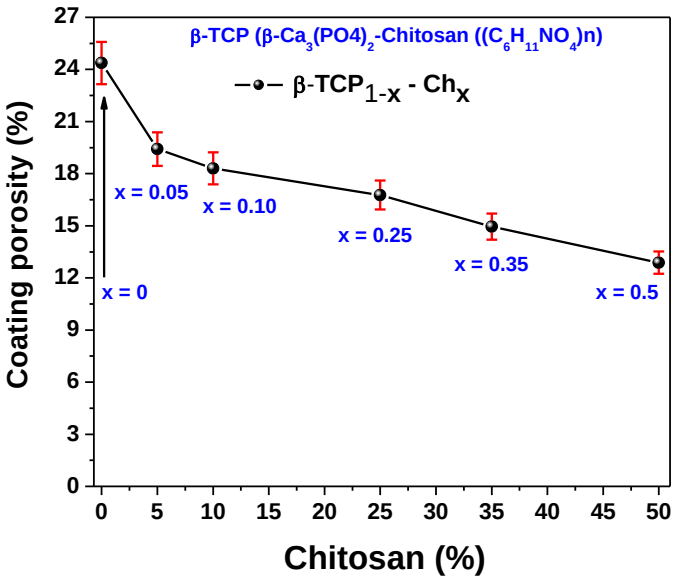

Figure 9. Coating porosity of β-TCP-Ch coating as function of Chitosan percentage

The protective efficiency of β-TCP-Ch coatings is a factor associated to surface nature and electrochemical nature; therefore, the protective efficiency factor can be determinate by using Eq. (3) the protective efficiency factor correspond to the ratio of the difference between corrosion intensity of the uncoated substrate and the corrosion intensity of coated substrate and corrosion intensity of the uncoated steel substrate [20], which in given bellow:

$$Ef(\%) = \left(\frac{I_{corr_S} - I_{corr_f}}{I_{corr_S}} \right) \times 100 \qquad (3)$$

where Ef is the total protective efficiency, I_{corr_s} is the corrosion intensity of the uncoated steel substrate, and I_{corr_f} is the corrosion intensity of the coated substrate.

Figure 10 efficiency factor values obtained are present, replacing the electrochemical values on Eq. (3) for each coating. The analysis of the curve suggests that the protective efficiency factor of β-TCP-Ch coatings is higher than AISI 316L stainless steel substrate, also with an increase of Chitosan percentage it can be possible observe an increase in values of protective efficiency. The results evidenced in Figure 10 are in agreement with corrosion results of EIS analysis of Fig 3.and polarization curves of Fig 7.

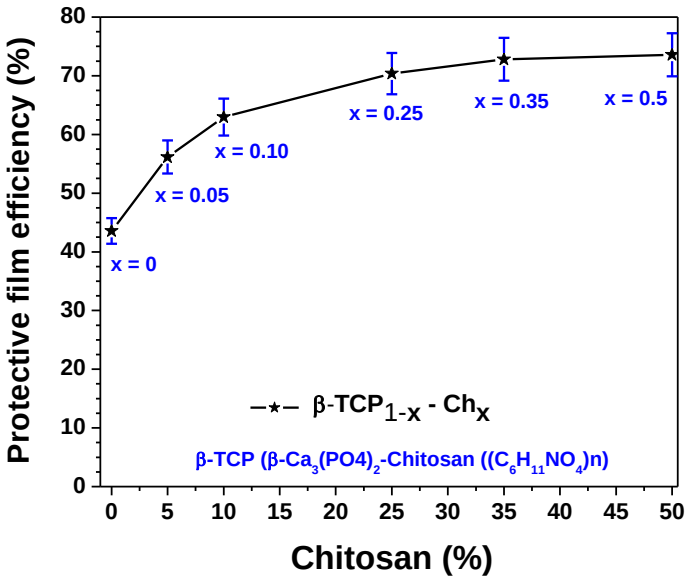

Figure 10. Protective film efficiency of β-TCP-Ch coatings as function of increase of Chitosan percentage.

3.5 Surface analysis after corrosive attack

The corrosive damage suffered by the coated samples with β-TCP_{1-x}-Ch_x materials, a microscopic analysis of the surfaces on the samples was conducted immediately after finishing the electrochemical measurements via scanning electron microscopy. Scanning electron microscopy (SEM) micrographs are shown in Fig. 11 for AISI 316L stainless steel substrate coated with β-TCP (β-$Ca_3(PO_4)_2$-Chitosan ($(C_6H_{11}NO_4)n$) under corrosion processes (Hanks solution) for different Chitosan percentage. When the Chitosan percentage is reduced to (0), Fig. 11a shows that a crack has been generated on the AISI 316l/β-TCP steel by wearing mechanisms, thus exhibiting a pitting corrosion with an intense corrosive delamination together with corrosion cracks. The dark areas reflect the surface damage caused by corrosion attack. Fig. 11b shows the AISI 316l/β-$TCP_{95\%}$-$Ch_{5\%}$ system with less wear damage compared to AISI 316l/β-TCP due to different microstructure and chemical

composition. Figs. 11c-f shows the surface of AISI 316L stainless steels substrate coated with the β-TCP_{1-x}-Ch_x without with lower corrosive delamination and corrosion cracks than that AISI 316l/β-TCP (Fig 11a), which exhibits the protection afforded by increasing of Chitosan percentage within coating system deposited on steel substrate such as AISI 316L/β-$TCP_{50\%}$-$Ch_{50\%}$ (Fig. 11f). These surface results are in agreement with coating porosity results (Fig. 9) and protective film efficiency results (Fig. 10).

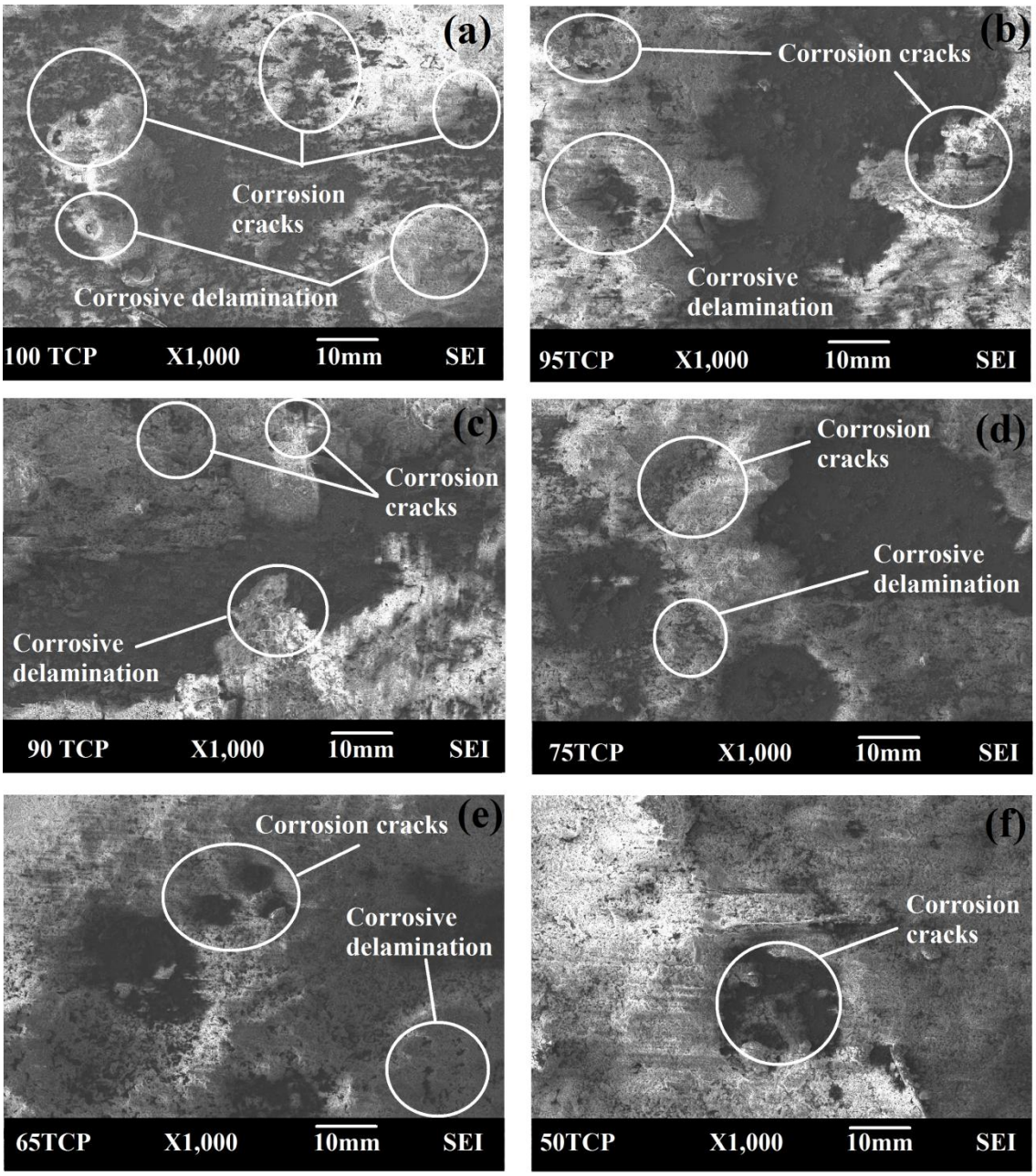

Figure 11. SEM micrographs for AISI 316L samples coated with β-TCP (β-$Ca_3(PO_4)_2$-Chitosan ($(C_6H_{11}NO_4)n$) under corrosion processes (Hanks solution) as function of increase of Chitosan percentage: (a) β-$TCP_{100\%}Ch_{0\%}$, (b) β-$TCP_{95\%}Ch_{5\%}$, (c) β-$TCP_{90\%}Ch_{10\%}$, (d) β-$TCP_{75\%}Ch_{25\%}$, (e) β-$TCP_{65\%}Ch_{35\%}$, and (f) β-$TCP_{50\%}Ch_{50\%}$.

3.5 EDS analysis after corrosive attack

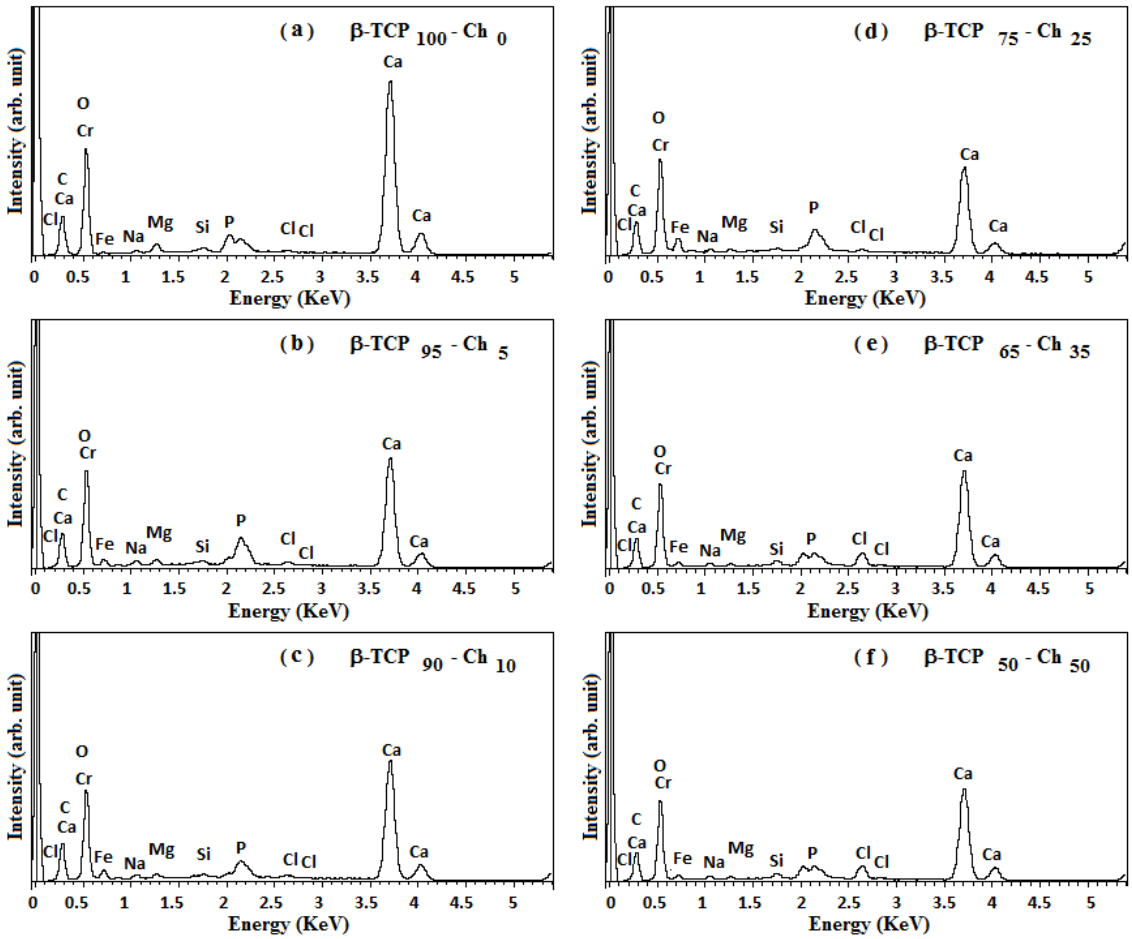

Figure 11. Energy dispersive X-ray spectroscopy (EDS) for β-TCP and β-TCP-Ch coatings as function of Chitosan concentration: (a) $\beta\text{-TCP}_{100\%}\text{Ch}_{0\%}$, (b) $\beta\text{-TCP}_{95\%}\text{Ch}_{5\%}$, (c) $\beta\text{-TCP}_{90\%}\text{Ch}_{10\%}$, (d) $\beta\text{-TCP}_{75\%}\text{Ch}_{25\%}$, (e) $\beta\text{-TCP}_{65\%}\text{Ch}_{35\%}$, and (f) $\beta\text{-TCP}_{50\%}\text{Ch}_{50\%}$.

Chemical analysis by using energy dispersive X-ray spectroscopy (EDS) was performed on the β-TCP (β-$Ca_3(PO_4)_2$-Chitosan ($(C_6H_{11}NO_4)n$) (β-TCP-Ch) coatings surfaces after finishing the electrochemical analysis to determinate possible chemical reaction in Hanks solution /surface coating interface; EDS spectra for each coating are shown in Figure 112; EDS spectra present preferential peaks of Chromium (Cr), Carbon (C) and Iron (Fe) elements associated with AISI 316L substrate, Also EDS spectra exhibit the constituent Calcium (Ca), Phosphorus (P), Oxygen (O) and Carbon (C) elements to confirm β-TCP and Chitosan existence. Finally, it was possible to observe preferential peaks associated to dissolved ions from Hanks solution acting on the coating surface; in this sense, EDS spectra indicate that both coatings were homogenous in composition and each one are reactive in Hanks solution.

Figure 112 indicates that an increase of Chitosan percentage could decrease values of intensity in preferential peaks of Calcium, Phosphorus, Oxygen and Carbon associated to β-TCP and Chitosan

materials due to a possible shielding of Chitosan that is mixed with β-TCP. On the other hand, EDS Spectra present also preferential peaks from Hanks solution ions (Mg^{+2}, Si^{+4} and Na^{+1}); that demonstrate the reactivity of β-TCP-Ch coatings with Hanks solution, due to biocompatible characteristics as bioactivity (due β-TCP) and cells proliferation (due Chitosan). Results obtained by EDS are associated with the improvement in electrochemical behavior due to bioactive characteristics of β-TCP and Ch materials analyzed by using EIS (Fig. 4) and Tafel curves (Fig. 7) and observed in SEM results (Fig. 11).

4. CONCLUSION

FTIR results indicate that the inclusion of Chitosan in β-Tricalcium phosphate (β-TCP (β-$Ca_3(PO_4)_2$)-Chitosan (($C_6H_{11}NO_4$)n) or ((Poly-(1-4)-2-Amino-2-deoxy-ß-D-Glucan) coating systems generate changes in β-TCP crystal lattice arrangement, it was evidenced by the increment in values of absorbance of vibration bands in FTIR spectra.

Electrochemical impedance spectroscopy results show that β-TCP-Chitosan coatings improve their electrochemical behavior while increase Chitosan percentage due to polymeric nature of polysaccharide. Also β-TCP-Ch coatings improve their values of polarization resistance while increase the exposition time under Hanks solution showing an increasing of 87% in the polarization resistance for β-$TCP_{50\%}Ch_{50\%}$.coating in relation to uncoated AISI 316L stainless steel substrate.

Tafel curves showed that β-$Ca_3(PO_4)_2$-($C_6H_{11}NO_4$)n (β-TCP-Ch) coatings present an excellent performance under aggressive solution such as Hanks solution, the coatings exposed decrease in corrosion rate due to bioactive characteristic of β-TCP material and polymeric nature of Chitosan material exhibits thus showing an reduction of 53% in the corrosion rate for β-$TCP_{50\%}Ch_{50\%}$.coating in relation to uncoated AISI 316L stainless steel substrate.

From electrochemical characterization was possible determinate an improvement n efficiency of β-TCP- Ch coatings and an increase of porosity factor related with the electrochemical performance of β-TCP-Ch coatings.

EDS results confirm the bioactive characteristic of β-TCP- Ch coatings and the reactivity of coating/Hanks solution interface due to existence of Hanks solution ions deposited on surface coating.

ACKNOWLEDGEMENTS
This work was supported by the Universidad Militar de Nueva Granada and the Universiad del Valle (EIMAT) Cali Colombia.

References

1. L. Lara, H. Estupiñan, D.Y. Peña, C. Vásquez, *Scientia et Technica*, 36 (2007) 273.
2. B. Ratner, A. Hoffman, F. Schoen, J. Lemons. *Biomaterials science: an introduction to materials in the medicine*, Academic press, San Diego, California, U.S.A (2006) .
3. Y. Abe, T. Kokubo and T. Yamamuro, *J Mater Sci Mater Med,* 1 (1990), 233.
4. B. G. Keselowsky, D. M. Collard, and A. J. García, *J Biomed Mater Res*, 66A (2003) 247.

5. Y. Liu; P. Layrolle, J. de Bruijn, C. van Blitterswijk, K. de Groot. *J. Biomed. Mater. Res*, 57 (2001) 327.
6. D. Peña, H. Estupiñan, H. Cordoba, C Vasquez, *Rev. Fac. Ing. Univ. Antioquia* 54, (2010) 15.
7. A. C. Tas and S. B. Bhaduri, *J Mater Res*, 19 (2004) 2742.
8. K. Teraoka, T. Nonami, Y. Doi, H. Taoda,K. Naganuma, Y. Yokogawa, T. Kameyama, *Materials Science and Engineering: C*. 13 (2000) 105.
9. X. Pang, I. Zhitomirsky. *Materials Chemistry and Physics*, 9 (2005) 245.
10. R. Martinez, H. Estupiñan, E. Cordoba, D. Peña, P. Anthony, M. Sundaram. Scientia et Technica, 36 (2007) 231.
11. K. Salma, L. Berzina-Cimdina, N. Borodajenko, *Processing and Application of Ceramics*, 4 (2010) 45.
12. R. Vani, E.K Girija, K. Elayuraja, S. Prakash, S. Parthiban. *J Mater Sci: Mater Med*. 20 (2009) 43.
13. B. Chen, Z. Zhaoquan. Z Jingxian, L. Qingling, J. Dongliang, *Materials Science and Engineering C*, 28 (2008) 1052.
14. U. Piratoba, E. Vera, C. Ortiz, *Dyna*. 162 (2010) 13.
15. J. E. B. Randles, Discuss. *Faraday Soc*., 1 (1947) 11.
16. N. Perez. *Electrochemistry and Corrosion Science*. Kluwer Academic Publishers (2004)
17. M. Stern, *Corrosion*, 14 (1958) 440.
18. W. Tato, D. Landolt, *J. Electrochem. Soc*. 145 (1998) 4173.
19. J. C. Caicedo, C. Amaya, G. Cabrera, J. Esteve, W. Aperador, M.E. Gomez, P. Prieto. *Thin Solid Films* 519 (2011) 6362.
20. J.C. Caicedo, G. Zambrano, W. Aperador, I. Escobar – Alarcon, E. Camps, *Applied surface* 256 (2011) 312.